Tel. No: +41 / 32 / 718 3257
Fax No: +41 / 32 / 718 3201
e-mail: nicolas.wyrsch@imt.unine.ch

Hydrogenated microcrystalline silicon for photovoltaic applications

N. Wyrsch[1], P. Torres[1], M. Goerlitzer[1], E. Vallat[1], U. Kroll[1], A. Shah[1], A. Poruba[2] and M. Vanecek[2]

[1]Institut de Microtechnique, University of Neuchâtel,
Breguet 2, 2000 Neuchâtel Switzerland.
[2]Institute of Physics, Academy of Sciences of the Czech Republic,
Cukrovarnicka 6, 16200 Prague 6, Czech Republic

Keywords: Microcrystalline, Silicon, Solar cells, Opto-electronic properties.

Abstract. Undoped hydrogenated microcrystalline silicon layers have been deposited by plasma CVD at low temperature at different power and silane dilution. Structural, optical and electrical properties of these layers have been investigated and are discussed in view of the deposition conditions. Entirely microcrystalline n-i-p solar cells have been deposited, incorporating the same layers as the intrinsic (i-) layer, in order to compare material and cell properties and identify the parameters important for photovoltaic applications.

Introduction

Hydrogenated microcrystalline silicon (μc-Si:H) deposited at *low temperatures* (< 300 °C) by *plasma Chemical Vapour Deposition* (CVD) has been known and used for more than 30 years. The first report on this material (sometimes also called "nanocrystalline" silicon, nc-Si:H) has been already published in 1968 [1] by Veprek et al. In the following years, Veprek and his co-workers have extensively studied μc-Si:H (deposited by chemical transport in hydrogen plasma) and published numerous and valuable papers (see [2, 3, 4, 5, 6] and citations within these papers). Despite this pioneering work, μc-Si:H never gained much interest for application as a photovoltaically active material in solar cells; it was, however, widely used for the doped layers of hydrogenated p-i-n solar cells, with hydrogenated amorphous silicon (a-Si:H) as the photo-active layer. One has to note that, in most cases, undoped μc-Si:H layers deposited by various groups exhibited a rather large n-type character (even without the use of doping gases), as well as large defect densities.

With the demonstration by our group of an entirely thin-film μc-Si:H p-i-n solar cell with an efficiency close to 5% [7], this material gained a renewed world-wide interest. Recently, stable efficiencies up to 8.5% have even been reported [8] for single junction p-i-n cells. The two key advantages of μc-Si:H (compared to a-Si:H) for its use in photovoltaic devices are: on one hand the enhanced infra-red light absorption and on the other hand the absence of light-induced degradation. This renders this material very interesting for use as the active layer of bottom cell of tandem or triple-junction thin-film silicon solar cells. Because it basically uses the same deposition technology as a-Si:H, μc-Si:H is an interesting candidate as a low band gap material in multi-junction cells and holds promise for low cost high-efficiency solar cells. Indeed, stable efficiencies in excess of 11% have been obtained by our group [9], by the research groups of Canon Corp. [10] and Kaneka Corp. [11]; in these cells a tandem structure consisting of an a-Si:H top cell and a μc-Si:H bottom cell was used. The latter group was also able to achieve 9.8% stable efficiency with a thin single-junction n-i-p poly-Si device (2.5 μm thick) [11]. However, this material was grown at notably higher temperatures (around 500 °C). Poly-Si p-i-n cells have also been grown by other

groups with the hot-wire technique (HW), but so far with only limited success [12, 13], as far as the cell results are concerned.

Despite the fairly extensive work invested in the study of plasma deposited μc-Si:H layers and cells, only limited knowledge exists on undoped (i.e. intrinsic or near intrinsic) "device-grade" material. The electronic transport mechanisms are not fully understood, and more specifically, the relation between material properties and cell performance is still not clear.

μc-Si:H material can be produced with numerous deposition techniques and under various deposition conditions. However, in this paper, we will reduce the scope to the properties of device grade μc-Si:H deposited by plasma enhanced CVD at temperatures around 200 °C, using the Very High Frequency Glow Discharge (VHF-GD) technique; since it is this kind of material which is at present incorporated in our own high-efficiency μc-Si:H solar cells [14]. The goal of this paper is to present an overview of the structural, optical and electrical properties of this type of μc-Si:H material and, specially, to discuss those of importance for photovoltaic devices. Some material and technological requirements will also be discussed. Finally, possible ways for the understanding of the electrical transport and its relation to solar cell performance will also be given.

Preparation

For photovoltaic applications, two important material properties must obviously be studied: light absorption and electronic transport. From the technological and economical point of view, the indirect band gap of μc-Si:H is a serious issue because, this means that thick diodes are basically required (leading, thus, to long deposition times) in order to get sufficient absorption. High deposition rate and effective light trapping scheme are therefore necessary. In our case, VHF-GD at frequencies between 110 and 130 MHz permits much higher deposition rates than the conventional RF-GD process [15, 16]. Furthermore, VHF-GD appears to be very beneficial for the microcrystalline growth [17, 16]. All layers presented in this paper were deposited at temperatures around 200 °C, with a concentration of silane in hydrogen varying between 1.25 and 7.5%. During deposition, a gas purifier has been used in order to avoid a too high incorporation of oxygen contaminants coming from the source gas. Similarly as in a-Si:H, but with a much more pronounced manner, oxygen in μc-Si:H acts as an effective n-type dopant [18], which rapidly tends to ruin the solar cell performance (see Fig. 1). Note, that this statement does not mean that a feedgas purifier is a paramount necessity, but rather that extra care must be taken to avoid oxygen contamination from the gas feed, as well as from the outgasing of the reactor.

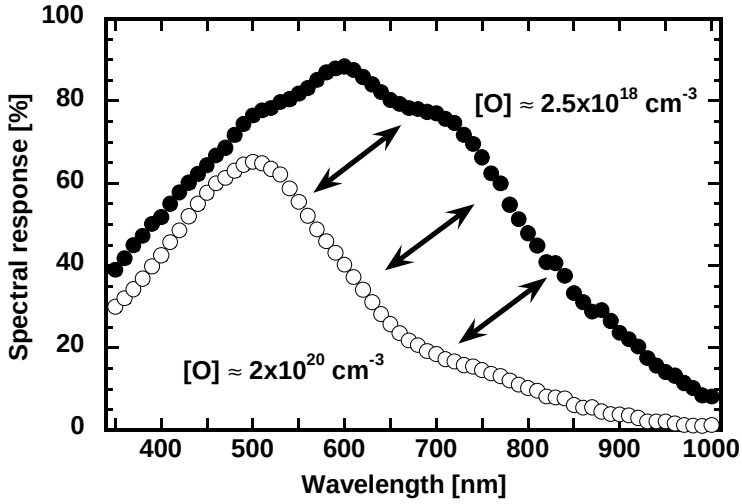

Fig. 1: Comparison of two entirely μc-Si:H cells, one deposited with (low oxygen content) and the other without (high oxygen content) a feedgas purifier. The cells are 2.8 μm thick and the oxygen content was measured by SIMS (Secondary Ion Mass Spectroscopy) in μc-Si:H layers deposited under the same conditions.

In this study we concentrated ourselves on two series of samples, deposited at 5% and at 7.5% concentration (of silane in hydrogen) at various deposition powers, at a plasma excitation frequency of 130 MHz. Undoped μc-Si:H layers, as well as entirely μc-Si:H cells incorporating these layers were fabricated and characterised. In order to understand the effect of silane concentration in hydrogen, a dilution series (with silane concentration between 1.25% and 7.5%) was also

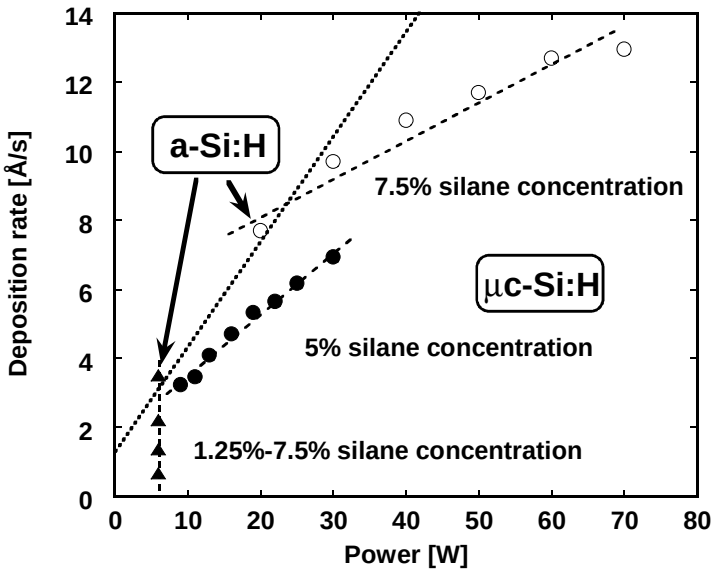

Fig. 2: Deposition rates obtained for the dilution series as well as the two power series (5% and 7.5% concentration). The transition between amorphous and microcrystalline growth is schematically indicated.

deposited at a fixed power (6 W) at 110 MHz. All cells were deposited on Asahi type U substrates (glass coated with textured SnO_2) in the n-i-p configuration and fitted with a top ITO (Indium Tin Oxide) top contact. The deposition rates obtained for all samples of these three series are indicated in Fig. 2. Note that all samples are microcrystalline with crystalline fractions over 80% (as determined by Raman spectroscopy) with the exception of the 7.5% concentration samples deposited at 6 W (of the dilution series) and the 20 W sample of the 7.5% concentration power series which are amorphous (see Fig. 2).

Structural properties

All of our µc-Si:H samples, deposited with the VHF deposition technique from a plasma of silane strongly diluted with hydrogen, exhibit a preferential growth in the [220] direction, as indicated by the X-ray diffraction (XRD) patterns plotted in Fig. 3. In most of the cases, this results in a columnar structure, which is clearly visible on a Scanning Electron Microscope (SEM) image, as shown on the right of Fig. 4. However, in some samples, for example the 5% concentration power series, such a columnar structure is not visible (Fig. 4, left). By monitoring the ratio of the (111) and the (220) peaks, one can determine the magnitude of this texture. While the 5% concentration power series shows an almost perfect [220] orientation, the 7.5% series exhibits a bell shaped curve with the most preferential growth observed around 50 W (see Fig. 5). For the dilution series, the preferential orientation decreases with increasing dilution. There is no simple relationship between the texture and the deposition parameters investigated here, i.e. silane dilution and plasma power (or the resulting deposition rate). On the other hand, it has been shown that these structural parameters (preferential orientation and columnar structure) can be controlled, in specific cases (for example using an argon and hydrogen dilution of silane), by the deposition conditions [19].

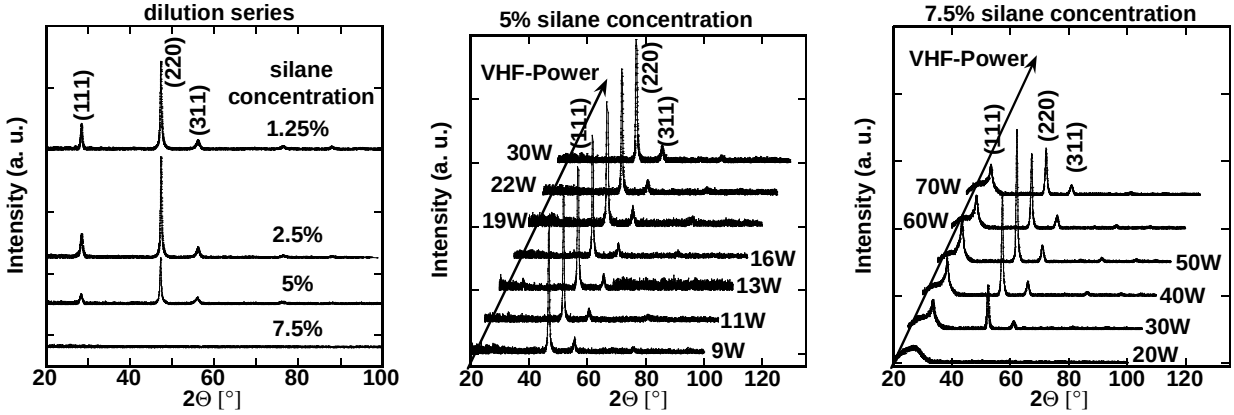

Fig. 3: X-ray diffraction patterns for samples of the dilution series, the 5% silane concentration power series and the 7.5% silane concentration series. For all µc-Si:H samples, a clear preferential growth along the [220] direction is observed.

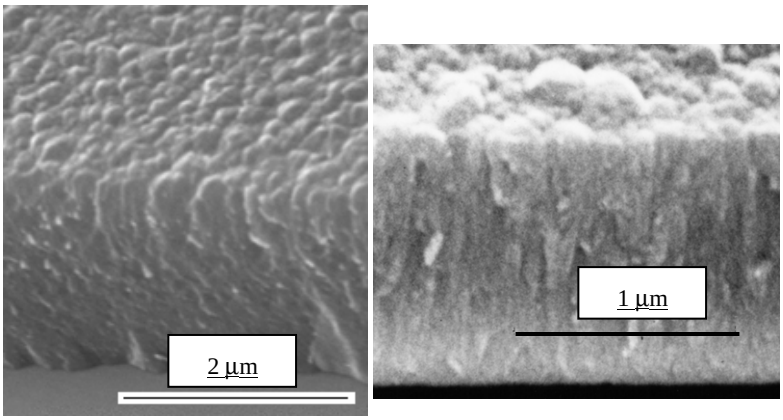

Fig. 4: SEM images of a µc-Si:H sample deposited at 5% concentration (of silane in hydrogen) and 11 W which shows no clear-cut columnar structure (left), compared with a typical µc-Si:H sample (deposited at a concentration of 2.5%, 70 MHz).

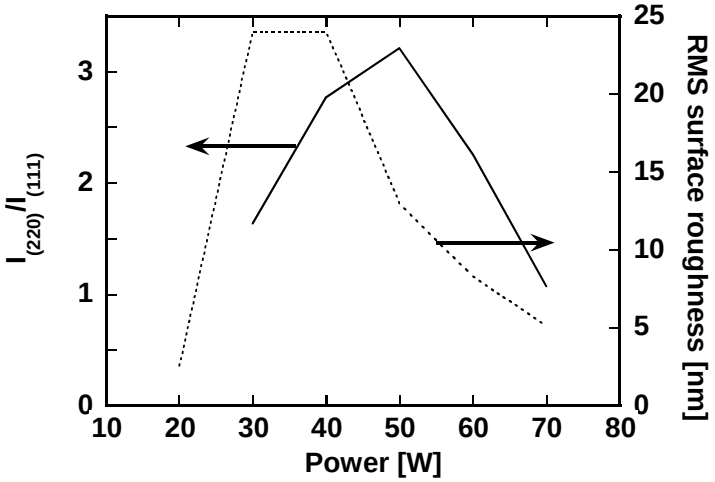

Fig. 5: Ratio of the intensities of the (220) and (111) diffraction peak, as well as the RMS surface roughness (obtained from a profilometer) as a function of deposition power for the 7.5% silane concentration power series.

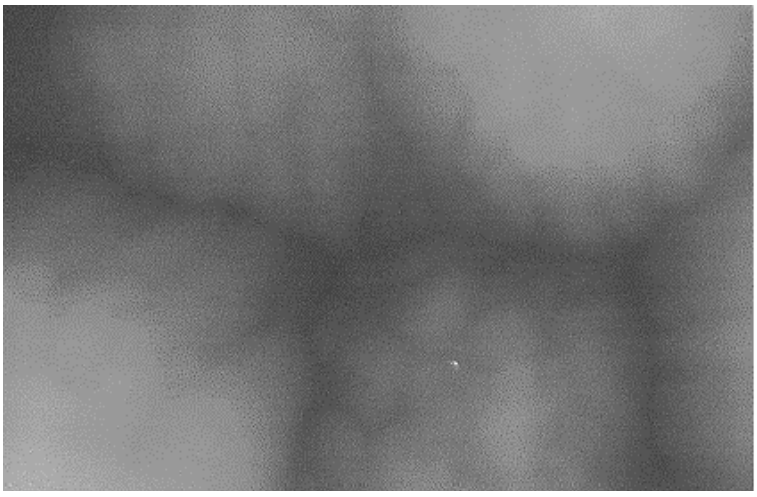

Fig. 6: Atomic Force Microscope image (1x0.6 µm) of a rough µc-Si:H film surface.

Using the Debye-Scherrer relation, one can try to extract the grain size from the width of the diffraction peak. Values obtained on our samples are all slightly above 200 Å, showing almost no dependence on the deposition power, and increasing only weakly with increasing dilution, up to 230 Å. The fact that the value of grain size remains almost constant over the investigated deposition parameter space is quite surprising, and contrasts with other published results [20, 21]. On the other hand, such low grain size values seem irreconcilable with the picture obtained from SEM. This could be attributed to the problem of XRD in reliably determining grain size using the Debye-Scherrer (the grain size can be severely underestimated) [22, 23].

Another important structural feature (that is specially important in connection with the light absorption, see section on optical properties) is the surface roughness observed usually on µc-Si:H. This surface roughness is quantified here by the variance of the height of surface points, as measured by a profilometer. The surface roughness tends to increase for increasing silane dilution (although the samples become less preferentially oriented), while for a given dilution (or concentration), it exhibits the same dependency in function of power as the preferential orientation (see Fig. 5). Increasing the deposition power tends to reduce the preferential growth along the [220] direction and produce a smoother surface. On some samples, especially on those exhibiting rough surfaces, the sub-

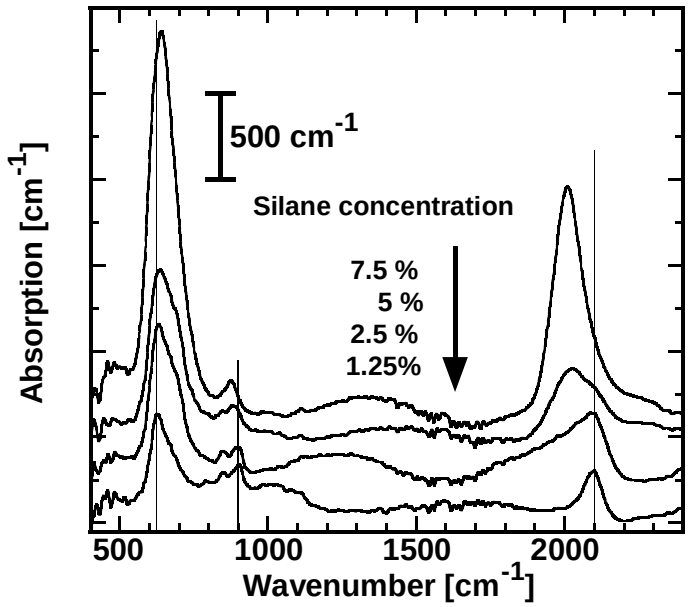

Fig. 7: Infrared absorption spectra of the dilution series. The vertical lines indicate the position of the peaks found in µc-Si:H (at 626, 900 and 2101 cm^{-1}). The 7.5% concentration sample exhibits typical a-Si:H behaviour.

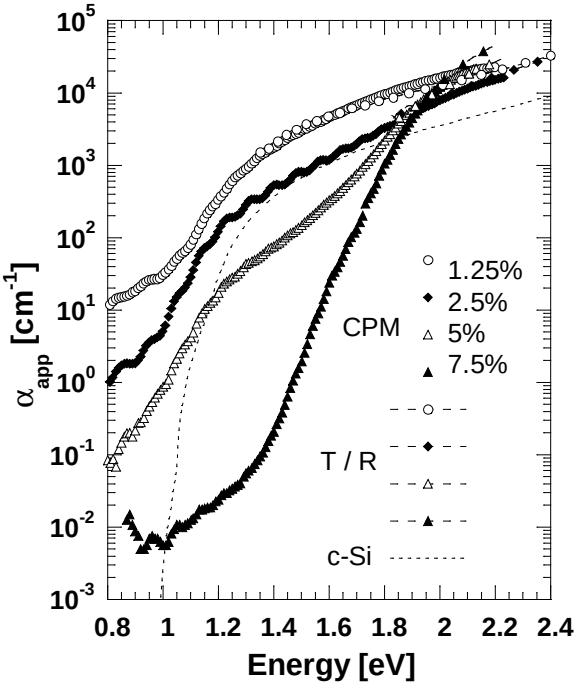

Fig. 8: Apparent optical absorption coefficient of the dilution measured by CPM and T/R (optical transmission/reflection). The transition from a-Si:H (7.5% silane concentration) to completely µc-Si:H material (2.5% and 1.25%) drastically changes the absorption spectra. The absorption coefficient of c-Si is given for comparison.

structure within the large columnar structure is clearly visible in AFM (Atomic Force Microscope) image (see Fig. 6). It is interesting to note here that the size of these substructures is in the range of 500 Å, and therefore they could be the coherence domains seen by XRD.

On Fig. 7, the infrared (IR) absorption spectrums of the dilution series are plotted. The 7.5% silane concentration sample exhibits the typical fingerprint of a-Si:H with peaks at 640, 840, 880, 2000 and 2090 cm^{-1} [24, 25]. After crossing the a-Si:H to µc-Si:H transition, new peaks appear at 626, 900 and 2101 cm^{-1}. The frequency shifts from the original a-Si:H positions is an indication for a change in the hydrogen bonding configuration. Following the results presented in Ref. [26, 27, 28, 29] these new vibrations modes can be assigned to mono and / or dihydride bonds on {100} and {111} surfaces of crystalline silicon. It therefore reflects the hydrogen bonded at the surface of crystalline grains. As far as the total hydrogen content is concerned, it drops sharply from 11% in a-Si:H to value around 5% in the µc-Si:H material. A more complete IR absorption study of the a-Si:H to µc-Si:H transition may be found in Ref. [30].

Optical properties

Following the transition from the amorphous to microcrystalline phase, we observe a shift of the absorption edge towards lower energies and a reduction of the absorption for energies >2 eV (see Fig. 8). This observation comes obviously from the reduction of the band gap of the material from 1.75 eV (a-Si:H) to 1.1 eV (c-Si) as well as from the change to an indirect band gap which drastically reduces the absorption in the visible. The 5% silane concentration power series exhibits similar absorption spectra (for all samples, see Fig. 9) as the high-dilution µc-Si:H samples in the dilution series. The enhanced absorption of µc-Si:H compared to c-Si is more surprising. The contribution to this enhanced absorption in the

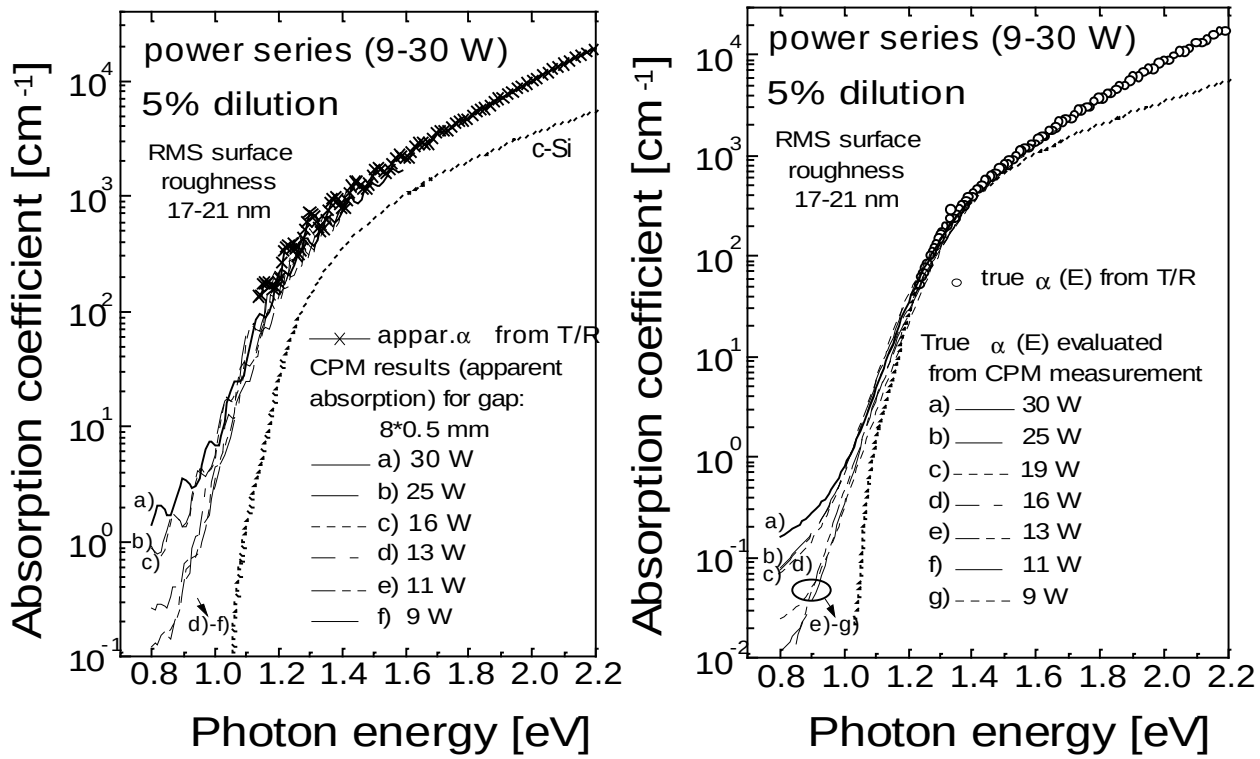

Fig. 9: Apparent absorption coefficient of the 5% silane concentration power series samples measured by CPM and T/R (left) as well as the true absorption for the same series (right). The surface roughness being constant for all samples in the 5% series, the differences in the apparent subgap absorption at 0.8 eV reflect directly the differences in defect density.

visible region can be mainly attributed to the residual amorphous fraction in the material. The situation in the IR region is more complicated. From CPM (Constant Photocurrent Method) measurements using different inter-electrode gaps, one can conclude that most μc-Si:H samples exhibit strong light scattering effects [31]. Thus, the latter has the effect of increasing the apparent thickness of the sample for scattered light, resulting in a measured apparent optical absorption coefficient that is significantly higher than the real true absorption of the material.

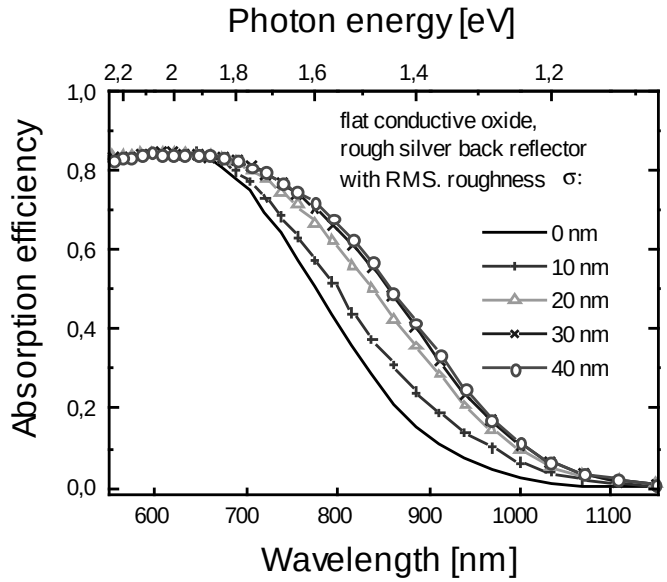

Fig. 10: Calculated spectral dependence of the absorption efficiency of a 3.5 μm thick μc-Si:H solar cell (in the glass-p-i-n configuration, with no antireflective coating) for different values of the RMS roughness of back reflector (given by the μc-Si:H surface texture).

This light scattering effect (which was already observed in some early films deposited by Veprek et al [3]) can be attributed almost entirely to the natural surface roughness of μc-Si:H layers. This has been demonstrated by the comparison of the true absorption of a rough μc-Si:H sample with the apparent absorption of the same sample after a chemomechanical polishing process (see Fig. 3 in Ref. 32). The two absorption curves being almost identical, it validates the optical

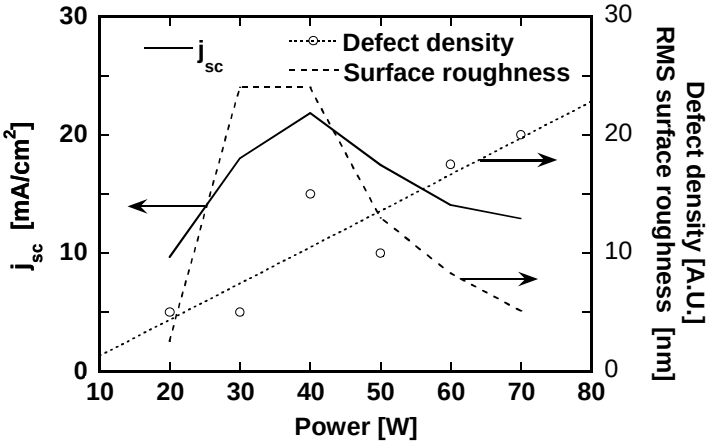

Fig. 11: Surface roughness, defect density (from CPM true absorption) of the 7.5% silane concentration power series, together with the short circuit current of corresponding solar cells (all with around 3.5 µm thickness). The maximum of the current (and a maximum efficiency of 5.2%) correlates with the maximum of the surface roughness.

modelling while confirming that most of the enhanced absorption in the IR region originates from the surface light scattering [32].

In order to deduce the defect density from the subgap absorption, one is interested in the "true absorption". This is done by first measuring the apparent absorption using the absolute CPM method [33], and then using an optical model, which takes into account the contribution of bulk and surface scattering [34], one can then calculate the true absorption. An example of the difference between apparent and true absorption is given on Fig. 9. The defect density of the best films is below 10^{15} cm^{-3}; it is obtained from the absorption coefficient at 0.8 eV of the best samples of Fig. 9 using the calibration factor given in Ref. 35. This low value is a good indication of the effective defect passivation by hydrogen.

For photovoltaic applications, this enhanced absorption by the surface light scattering is useful, because it helps increase the effective cell thickness: One can obtain higher currents, or, alternatively, one can reduce the actual thickness (and the deposition time) while obtaining the same current. An theoretical example is given in Fig. 10, which shows the effect of the hypothetical back reflector texture (as given e.g. by the surface roughness of the deposited µc-Si:H cell) on the absorption efficiency within the cell. A practical example is given in Fig. 11. Here (for the 7.5% silane concentration power series), the maximum current (with a corresponding efficiency of 5.2%) is obtained for one of the highest surface roughness. Note that the highest efficiency of 6.5% is obtained in the 5% series for the 22 W sample, a sample that has lower surface roughness, but also a much lower defect density and a more pronounced intrinsic character (see Fig. 12).

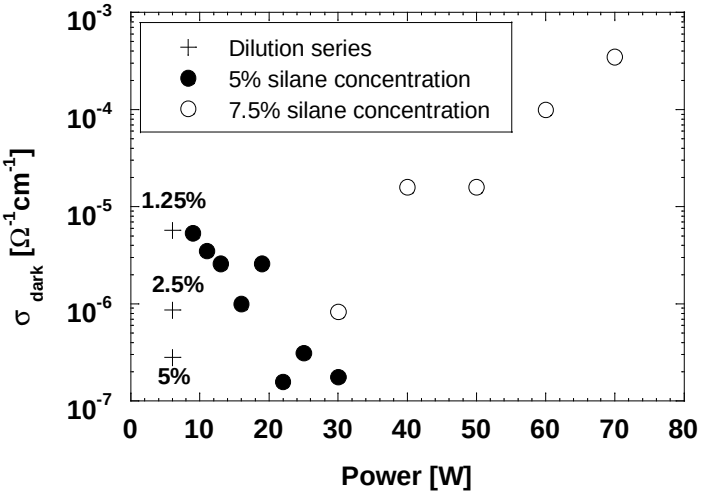

Fig. 12: Dark conductivity as a function of deposition power and silane concentration for the dilution series and for the 5% and 7.5% silane concentration power series (only µc-Si:H samples are plotted here).

Electrical properties

As already mentionned above in the section on preparation, µc-Si:H samples exhibit in most of the case a n-type behaviour due to the *incorporation of oxygen* atoms during growth. In general, we observe a decrease in the oxygen content in the film with increasing deposition rate; the decrease in

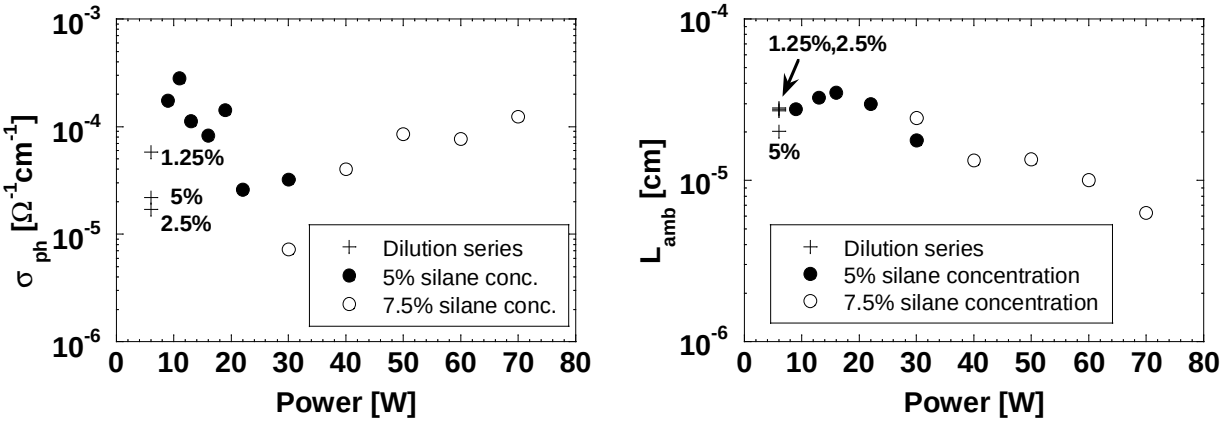

Fig. 13: Photo-conductivity (left) and ambipolar diffusion length (right) as a function of deposition power and silane concentration for the dilution series and for the power series with 5% and 7.5% silane concentration (the values of the two a-Si:H samples within these series are omitted here). Samples are measured at a generation rate of G≈1.5x10^{20} cm^{-3}s^{-1}.

oxygen content induces a decrease in the dark conductivity σ_{dark} and an increase in the latter's activation energy. One source of oxygen contaminents is the outgasing of the reactor itself. Because this oxygen flux is independent of deposition rate, it results in oxygen incorporation in the μc-Si:H layer which is deposition-rate dependent. However, in the case of Fig. 12, this mechanism only explains the results observed for the dilution series. For the 5% silane concentration series, the oxygen content is for all samples between 3x10^{18} and 7x10^{18} cm^{-3} (measured by SIMS) and does not correlate with the deposition rate; σ_{dark} depends rather on the defect density (see Fig. 9). The case of the 7.5% is more complicated. In this series, σ_{dark} is strongly influenced by the oxygen content which varies from 3x10^{19} (20 W sample) to 7x10^{18} cm^{-3} (70 W sample). At these very high level of oxygen contamination, it is quite surprising that corresponding cells incorporating the same i-layer can still behave satisfactorily (see Fig. 11). This could indicate that oxygen in these layers is mainly due to a strong post-deposition oxydation effect (see also below), an effect that modified drastically also the dark conductivity. Note that such post-oxydation is not observed in p-i-n (or n-i-p) solar cells, because the i-layer is sealed off by the doped and contact layers [9].

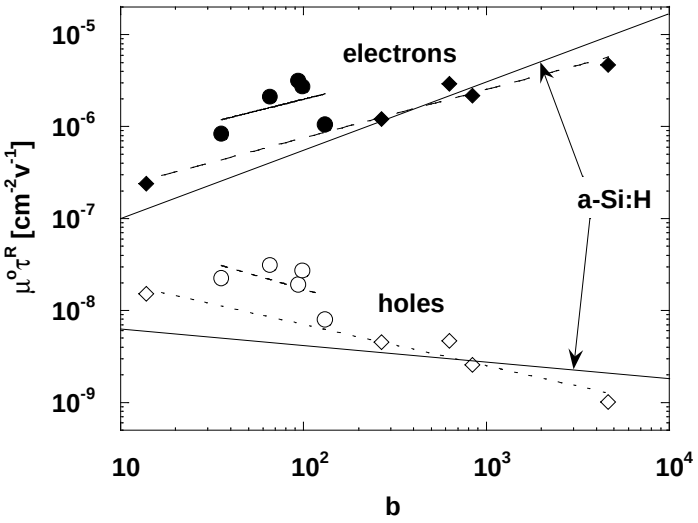

Fig. 14: Mobility x recombination time for electrons and holes as a function of the parameter b for the 5% (circles) and 7.5% (diamonds) silane concentration power series. Samples are measured at generation rate G≈1.5x10^{20} cm^{-3}s^{-1}. The parameter $b = (\mu_n^0 n)/(\mu_p^0 p)$ is used here to describe the position of the Fermi level (b=1 in case of a fully intrinsic layer). For a-Si:H (the typical behaviour is shown here for comparison), samples with b<50 may be considered intrinsic.

Fig. 13 shows measured values of the photo-conductivity σ_{ph} and of the ambipolar diffusion length L_{amb}, measured by SSPG (Steady-State Photocarrier Grating), for the same three series of samples. The variations observed here are indeed those that one would expect from the change of

the dark conductivity (or of its activation energy): a more intrinsic sample leads to a lower photo-conductivity and a higher ambipolar diffusion length. In order to represent more clearly this effect of the Fermi level position, one can plot σ_{ph} and L_{amb}, as a function of the Fermi level position, or more conveniently, as a function of the parameter b (Fig. 14). This parameter $b = (\mu_n^0 n)/(\mu_p^0 p)$ can be derived from the measurement of σ_{ph}, L_{amb} and generation rate G, according to a procedure given in [36] and applied there to the case of a-Si:H sample; b is approximately 1 for an intrinsic sample. As observed in Fig. 14, the values obtained for σ_{ph} and for L_{amb}, are closed to those observed for a-Si:H layers. However, in contrast with a-Si:H, the ambipolar diffusion length L_{amb} of μc-Si:H samples shows almost no dependence on the generation rate, while σ_{ph} behaves similarly as in a-Si:H; it follows a power law with an exponent between 0.5 and 0.85 [36]. Furthermore, one should also note that no light-induced degradation is observed in these μc-Si:H layers even under strong illumination [37].

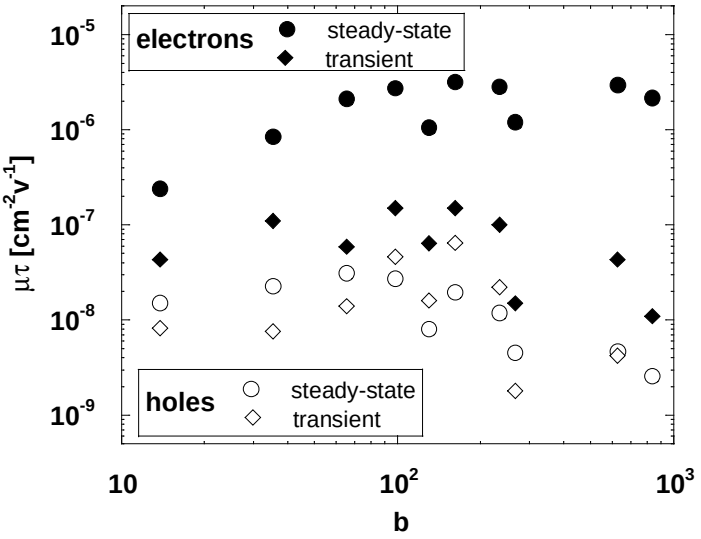

Fig. 15: Comparison of the steady-state and transient mobility x life time products for electrons and holes as a function of the parameter b for the 5% and 7.5% silane concentration power series. Steady-state values are calculated from the photo-conductivity and ambipolar diffusion length (at the generation rate $G \approx 1.5 \times 10^{20}$ $cm^{-3}s^{-1}$), while transient values are measured with TOF.

Table I: Drift mobilities for electrons and holes measured by TOF for the dilution series. The 7.5% sample is amorphous.

Silane concentration [%]	μ_n^D [cm^2/Vs]	μ_p^D [cm^2/Vs]
1.25	2.9	1.1
2.5	1.5	1.0
5	1.2	0.41
7.5	0.91	0.011

For a material with a columnar structure or a preferential growth, σ_{ph} and L_{amb}, which are measured in coplanar configuration, basically do not reflect the transport properties relevant to solar cells (with a sandwich configuration). Therefore, it is important to also characterise the transport in the direction perpendicular to the substrate. For this purpose, the *time of flight (TOF) technique* was used to extract drift mobilities (Table I) and mobility x lifetime products (Fig. 15), for both electrons and holes. Compared to a-Si:H, μc-Si:H samples exhibit electron mobilities which are only a factor of 2-3 higher, and increasing with increasing dilution. On the other hand, μc-Si:H drift mobilities for holes are much higher than those of a-Si:H. As far as the mobility x lifetime ($\mu\tau$) products are concerned (Fig. 15), one observes for the 5% and 7.5% series the same behaviour as prevailing in a-Si:H [38]: for the majority carriers (electrons), the steady-state $\mu\tau$ products (as derived from σ_{ph}) are about 10 times larger than the transient $\mu\tau$ products (as derived from TOF), while the corresponding values for the $\mu\tau$ products of minority carriers (holes) are similar. This observation leads to the hypothesis that the structural anisotropy in these μc-Si:H layers

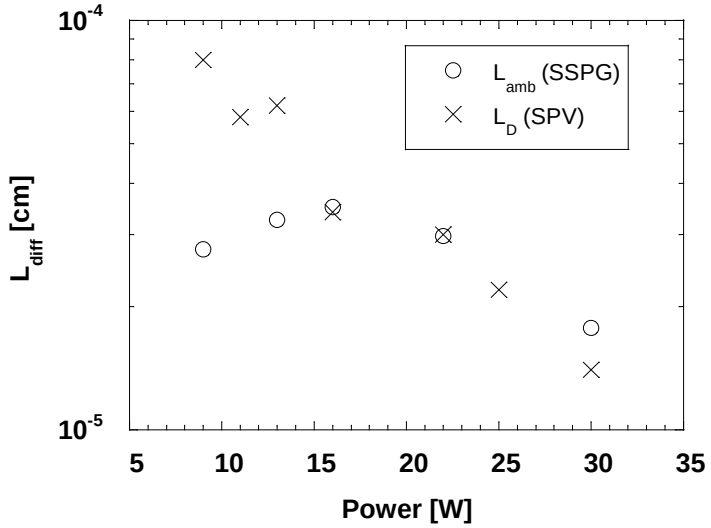

Fig. 16: Comparison between the diffusion length measured by SPV and the ambipolar diffusion length measure by SSPG) (at the generation rate G≈1.5x10^{20} $cm^{-3}s^{-1}$).

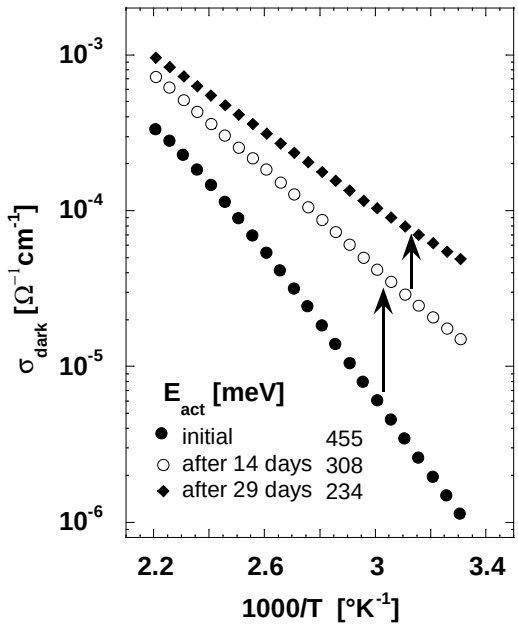

Fig. 17: Change of the dark conductivity and activation energy with time due to the post-oxidation in air of µc-Si:H sample grown at 5% silane concentration and 10 W.

does not translate in a significant anisotropy of the transport properties.

As a further check of this hypothesis, diffusion lengths L_D were measured by SPV (Surface Photo-Voltage) on samples of the 5% power series and compared with the values of L_{amb} obtained from SSPG. Note that L_D (SPV) evaluates diffusion length in a direction perpendicular to the substrate (sandwich configuration) whereas L_{amb} (SSPG) evaluates diffusion lengths in direction parallel to the substrate (coplanar configuration). Fig 16. shows that L_D and L_{amb} are almost equal for high power samples, indicating little anisotropy in diffusion. On the other hand, some anisotropy can be found for the small power samples. One should also note that L_D correlates nicely with the defect density (see Fig. 9); L_D is inversely proportional to the defect density. These results indicate that an anisotropy seems to exist for the low power samples. An anistropy in the transport properties for the same series of sample was also suggested by Kocka et al from an analysis of AC conductivity data [39].

As already mentioned above, µc-Si:H samples tend to exhibit post-deposition oxidation. This general feature of most (if not all?) µc-Si:H samples has already been documented in Refs. [4, 5, 9, 40]. One observe that this oxidation is a volume process, with a gradient of oxygen going deep into the sample, but with a magnitude which can change from sample to sample, and therefore could be possibly controlled [40]. One fingerprint of this process is a drastic change in the dark conductivity and its activation energy (see Fig. 17). In case of strong oxidation, peaks related to Si-O bonds may also appear in the IR absorption spectrum. This post-oxidation effect, which causes a serious problem for the characterisation of the layers, is observed not to affect cells, probably because the active i-layers are sealed off by the doped and contact layers [9]. Because of this post-oxidation effect, layers characterisation should always be carried out simultaneously with a careful evaluation of the Fermi level position (for example by determining the parameter b).

Summary

For a few years, undoped µc-Si:H (deposited at temperatures below 300 °C) has been very successfully used thin film solar cells. In this context, its low gap, enhanced absorption (compared to c-Si) and stability with respect to light-soaking are the attractive features of this material. However, due to the structural nature µc-Si:H (crystallites of various sizes and orientations embedded in a residual amorphous tissue), the study of this material is complex. Furthermore, µc-Si:H can be deposited under many different conditions and the deposition conditions affect quite drastically the structure.

In this study, we deliberately concentrate ourselves on device-grade µc-Si:H layers, actually used in solar cells (entirely µc-Si:H p-i-n with efficiency up to 6.5%). From the structural, optical and electrical characterisation of these layers, one can draw three observations. First, µc-Si:H structure can be changed over a very wide range by tuning the deposition conditions but we do not know at this point what is the "optimum" structure for the best solar cell. Second, a rough (textured) µc-Si:H surface is certainly a desirable feature in order to improve the IR absorption, but we have to be sure that the transport is not affected. Third, it is quite puzzling to see how the transport in µc-Si:H is similar to the one in a-Si:H. So far the it still lacks a comprehension of its mechanism. The model of Seto [41], which has been widely used for poly-Si, is physically unsatisfactory due to the low defect density and low grain size of µc-Si:H. Percolation models have also been proposed [21], but it is up to now not clear if they can be applied to all type of µc-Si:H and more specifically to device grade intrinsic µc-Si:H. In solar cells, it is also not clear what are the transport mechanisms controlling their functioning, even though there are indication that both drift and diffusion processes are involved [42]. However, best material for solar cells should at least exhibit a low defect density, intrinsic character (and therefore low oxygen content) and a high surface roughness.

Acknowledgments

This work was supported by the Swiss Federal Renewable Energy Program (grant 19431) and the Swiss National Foundation grant FN-45696 and FN-52337.

References

[1] S. Veprek, V. Marecek, Solid-State Electron. **11**, 683 (1968).
[2] S. Veprek, Z. Iqbal, H.R. Oswald, A.P. Webb, J. Phys. C **14**, 295 (1981).
[3] Z. Iqbal, F.-A. Sarott, S. Veprek, J. Phys. C **16**, 2005 (1983).
[4] S. Veprek, Z. Iqbal, R.O, Kühne, P. Capezzuto, F.-A. Sarott, J.K. Gimzewski, J. Phys. C **16**, 6241 (1983).
[5] H. Curtins, S. Veprek, Sol. State Comm. **57**, 215 (1986).
[6] S. Veprek, M. Heintze, F.-A. Sarott, M. Jurcik-Rajman, P. Willmott, Mat. Res. Soc. Symp. Proc. **118**, 3 (1988).
[7] J. Meier, R. Flückiger, H. Keppner, A. Shah, Appl. Phys. Lett. **65**, 860 (1994).
[8] J. Meier, S. Dubail, L. Feitknecht, Y. Ziegler, P. Torres, C. Hof, U. Kroll, D. Fischer, J. Cuperus, H. Keppner, A. Shah, *Proc. of the 2nd World Conf. on Photovoltaic Solar Energy Conversion*, Vienna, 1998, in print.
[9] J. Meier, S. Dubail, J. Cuperus, U. Kroll, R. Platz, P. Torres, J.A. Anna Selvan, P. Pernet, N. Beck, N. Pellaton Vaucher, C. Hof, D. Fischer, H. Keppner, A. Shah, J. of Non-Cryst. Sol. **227-230**, 1250 (1998).
[10] K. Saito, M. Sano, K. Matuda, T. Kondo, T. Nishimoto, K.Ogawa, I. Kajita, *Proc. of the 2nd World Conf. on Photovoltaic Solar Energy Conversion*, Vienna, 1998, in print.
[11] K. Yamamoto, M. Yoshimi, T. Susuki, Y. Okamoto, Y Tawada, A. Nakajima, *Proc of the 26th IEEE Photovoltaic Specialist Conference*, 575 (1997).

[12] J.K. Rath, A.J.M.M van Zutphein, H. Meiling, R.E.I. Schropp, Mat. Res. Soc. Symp. Proc. **467**, 445 (1997).
[13] A.R.Middya, J. Guillet, R. Brenot, J. Perrin, J.E.Bourree, C. Longeaud, J.P. Kleider, Mat. Res. Soc. Symp. Proc. **467**, 271 (1997).
[14] P. Torres, J. Meier, U. Kroll, N. Beck, H. Keppner, A. Shah, *Proc of the 26th IEEE Photovoltaic Specialist Conference*, 711 (1997).
[15] F. Finger, P. Hapke, R. Carius, H. Wagner, Appl. Phys. Lett. **65**, 2588 (1994).
[16] P. Torres, J. Meier, R. Flückiger, H. Keppner, A.Shah, Mat. Res. Soc. Symp. Proc. **452**, 767 (1997).
[17] H. Hapke, F.Finger, M. Luysberg, R. Carius, H. Wagner, Mat. Res. Soc. Symp. Proc. **358**, 745 (1995).
[18] P. Torres, J. Meier, R. Flückiger, U. Kroll, J. A. Anna Selvan, H. Keppner, A. Shah, S.D. Littlewood, I.E. Kelly, P. Giannoulès, Appl. Phys. Lett. **69**, 1373 (1996).
[19] H. Keppner, U. Kroll, P. Torres, J. Meier, R. Platz, D. Fischer, N.Beck, S. Dubail, J. A. Anna Selvan, N. Pellaton Vaucher, M.Goerlitzer, Y. Ziegler, R. Tscharner, Ch. Hof, M. Goetz, P. Pernet, N. Wyrsch, J. Vuille, J. Cuperus, A. Shah, J. Pohl, Mat. Res. Soc. Symp. Proc. **452**, 865 (1997).
[20] A. Matsuda, K. Kumagai, K. Tanaka, Jpn. J. Appl, Phys. **22**, L34 (1983).
[21] R. Carius, F. Finger, U. Backausen, M. Luysberg, P. Habke, L. Houben, M. Otte, H. Overhof, Mat. Res. Soc. Symp. Proc. **467**, 283 (1997).
[22] B.D. Cullity, in *Elements of X-Ray Diffraction* (Addison-Wesley Publishing Company, Inc, 1978), p 283.
[23] S. Veprek, F.-A. Sarott, M. Rückschloss, J. Non-Cryst. Sol. **137&138** 733 (1991).
[24] M.H.Brodsky, M. Cardona, J.J. Cuomo, Phys. Rev B **16**, 3556 (1977).
[25] G. Lukovsky, R.J. Nemanich, J.C. Knights, Phys. Rev B **19**, 2064 (1979).
[26] H. Wagner, W. Beyer, Sol. State Comm. **48**, 587 (1983).
[27] Y.J. Chabal, E.E. Chaban, S.B. Christman, J. Electron Spectr. Rel. Phenom. **29**, 35 (1983).
[28] Y.J. Chabal, Phys. Rev. Lett. **50**, 1850 (1983).
[29] T. Saitoh, A. Hiraki, Jpn. J. Appl. Phys. **24**, L491 (1985).
[30] U. Kroll, J. Meier, P. Torres, J. Pohl, A. Shah, J. of Non-cryst. Sol. **227-230**, 68 (1998).
[31] N. Beck, J.Meier, J. Fric, Z. Remes, A. Poruba, R. Flückiger, J. Pohl, A. Shah, M. Vanecek, J. of Non-cryst. Sol. **198-200**, 903 (1996).
[32] A. Poruba, Z. Remes, J. Springer, M. Vanecek, A. Fejfar, J. Kocka, P. Torres, A. Shah, *Proc. of the 2nd World Conf. on Photovoltaic Solar Energy Conversion*, Vienna, 1998, in print.
[33] M.Vanecek, J. Kocka, A. Poruba, A. Feijfar, J. Appl. Phys. **78**, 6203 (1985).
[34] A. Poruba, Z. Remes, A. Feijfar, J. Kocka, M. Vanecek, to be published.
[35] N. Wyrsch, F. Finger, T.J. McMahon, M. Vanecek, J of Non-cryst. Sol. **138&138**, 347 (1991).
[36] M. Goerlitzer, N. Beck, P. Torres, J. Meier, N. Wyrsch, A. Shah, J. Appl. Phys. **80**, 5111 (1996).
[37] M. Goerlitzer, N. Beck, P.Torres, U. Kroll, H. Keppner, J. Meier, J. Koehler, N. Wyrsch, A. Shah, Mat. Res. Soc. Symp. Proc. **467**, 301 (1997).
[38] N. Beck, N. Wyrsch, E. Sauvain, A. Shah, Mat. Res. Soc. Symp. Proc. **297**, 479 (1993).
[39] J. Kocka, A. Fejfar, H. Stuchlikova, B. Rezek, A. Poruba, M. Vanecek, P. Torres, J. Meier, N. Wyrsch, A. Shah, A. Matsuda, *Proc. of the 2nd World Conf. on Photovoltaic Solar Energy Conversion*, Vienna, 1998, in print.
[40] M. Goerlitzer, P. Torres, N. Beck, N. Wyrsch, U. Kroll. H. Keppner, J. Pohl, A. Shah, J. of Non-cryst. Sol. **227-230**, 996 (1998).
[41] J.Y.W. Seto, J. Appl. Phys. **46**, 5247 (1975).
[42] N. Wyrsch, P.Torres, J. Meier, A. Shah, J. of Non-cryst. Sol. **227-230**, 1272 (1998).